

Inversion and magnetization homogeneity testing for 2D magnetic sources

William Pareschi Soares¹ and Carlos Alberto Mendonça²

ABSTRACT

Many approaches to magnetic data inversion are based on assumptions that source magnetization is homogeneous in direction and intensity. Such assumptions rarely can be verified with independent geologic information and are usually incorporated without further inquiry in the next steps of data interpretation. The use of magnetization direction invariants, such as the gradient intensity of the total field anomaly (equivalent to the amplitude of the analytical signal [ASA]) and the intensity of the anomalous vector field (IAVF), is effective for modeling sources with strong remanent magnetization, usually with unknown direction. Even in such cases, however, the assumption of uniform magnetization is understood but unchecked when seeking smooth or compact solutions from data inversion. We have developed a procedure to test the assumption of uniform magnetization for 2D sources. For true 2D homogeneous sources, the ratio of ASA to IAVF can be modeled with a binary solution (0 and 1) regardless of the real value of the magnetization. A procedure to provide convergence was applied, and its output solution was submitted to a binary test to verify the uniformity hypothesis. This technique was illustrated with numerical simulations and then used to reinterpret a ground magnetic profile across an intrusive diabase body in sediments of the Paraná Basin, Brazil, revealing the existence of two adjacent bodies that are homogeneous with different magnetization intensities.

INTRODUCTION

The quantitative interpretation of magnetic data using inversion procedures is an ill-posed problem (Tikhonov and Arsenin, 1977) requiring specific regularization procedures to suit solutions with uniqueness and stability. The introduction of a priori information

based on available geologic data defines a realistic scenario to obtain reliable representations for the subsurface geology. The available information must be translated as mathematical expressions of regularizing functionals to be effectively incorporated in the data inversion (Silva et al., 2001). In many cases, however, the databases for physical properties and attributes of geologic entities are limited to outcrops and borehole information, usually lacking sufficient coverage to provide quantitative constraints for the entire geologic structure. The constraints incorporated in the data inversion then tend to guarantee the general attributes expected for geologic formations, usually in terms of smooth variations in physical properties (Barbosa and Silva, 1994) or compact (minimum volume) distributions (Last and Kubik, 1983; Portniaguine and Zhdanov, 2002), for example.

For magnetic sources with strong remanent magnetization, the inversion of the total field anomaly (TFA), which is highly dependent on the magnetization direction, has been substituted by the inversion of field intensities that are invariant (for 2D sources) with the magnetization direction (Liu et al., 2013, 2015). For 3D sources, such intensity fields are not invariant with the magnetization direction but are less sensitive than TFA (Shearer and Li, 2004; Li et al., 2010, 2018; Li and Pilkington, 2016), easing the representation of underlying sources by assuming an arbitrary magnetization direction. Most popular invariant or less-sensitive intensity fields are the intensity of the anomalous vector field (IAVF) (Li et al., 2010; Liu et al., 2013) and the amplitude of the analytical signal (ASA) (Shearer and Li, 2004; Li and Pilkington, 2016), which is equivalent to the gradient intensity of the TFA. Inversion of the ASA was introduced by Shearer and Li (2004). Later works point out advantages for the IAVF inversion because of its higher sensitivity to greater depth when compared with ASA, which is more sensitive to upper levels (Li et al., 2010; Liu et al., 2013, 2015). Nonlinear field quantities less sensitive to the magnetization direction have been proposed to improve source location in gridded data sets (Stavrev and Gerovska, 2000; Stavrev, 2006), but they are not incorporated in formulations based on data inversion.

Another way to overcome the lack of knowledge about the magnetization intensity and direction is to invert the ratio between com-

Manuscript received by the Editor 18 June 2019; revised manuscript received 11 September 2020; published ahead of production 13 October 2020; published online 07 January 2021.

¹IFSP-Federal Institute of São Paulo, Rua Ten. Miguel Délia, 105, São Paulo, Brazil. E-mail: william.soares@ifsp.edu.br (corresponding author).

²IAG-USP, Rua do Matão 1226, São Paulo, Brazil. E-mail: camendonca@usp.br.

© 2020 Society of Exploration Geophysicists. All rights reserved.

ponents and field intensities. For uniform sources, the evaluation of such ratios cancels the magnetization intensity, hence allowing shape reconstruction and depth estimates without requiring previous knowledge on the magnetization intensity. The tilt angle technique (Wijns et al., 2005; Salem et al., 2008; Hidalgo-Gato and Barbosa, 2015) can be regarded as a successful case of a ratio-based technique to accurately outline geologic contacts and depth to the top for contact or thin sheet models. There are few cases in which ratio quantities are inverted for more complex (polygonal) sources (Mendonça, 2004; Tuma and Mendonça, 2007).

Another characteristic of inversion methods incorporating invariants is the adoption of sequential or stepped procedures in which the inversion of the TFA is postponed once a solution from inverting intensity fields or ratios is provided. The sequential inversion of Liu et al. (2015) initially inverts IAVF to outline the source geometry, which is then used as the input to fit the TFA. The stepped inversion of Tuma and Mendonça (2007) sequentially inverts the shape function (SF) to determine the geometry of the sources, next to determine the magnetization intensity with ASA inversion, and finally to determine the magnetization inclination by fixing previous estimates and fitting the TFA. Low convergence rates in inverting the SF prevented advance to the next steps, especially for highly heterogeneous sources for which no uniform solution exists.

We present a procedure that postpones the inversion of a ratio quantity to a later stage of a sequential procedure to allow model convergence and analysis of the obtained solutions. The sources are represented by a mesh of juxtaposed cells to represent sources with complex geometry. The test for uniform magnetization is applied once having a solution fitting the ASA, IAVF, and SF. This approach reverses the order in which the stepped inversion was applied and introduces a simple binary constraint to test the uniformity of the source. Our technique was tested with numerical simulation and then used to reinterpret a ground magnetic profile already modeled with a set of adjacent vertical prisms (Tuma and Mendonça, 2007).

THEORETICAL ASPECTS

The TFA measured along a profile transverse to a magnetic structure can be grouped into a data vector \mathbf{f}_t , the subscript t denoting the direction \mathbf{t} of the local main field. This data vector has entries $f_{t,i}$, for readings at positions x_i , $i = 1:n$. The distribution of magneti-

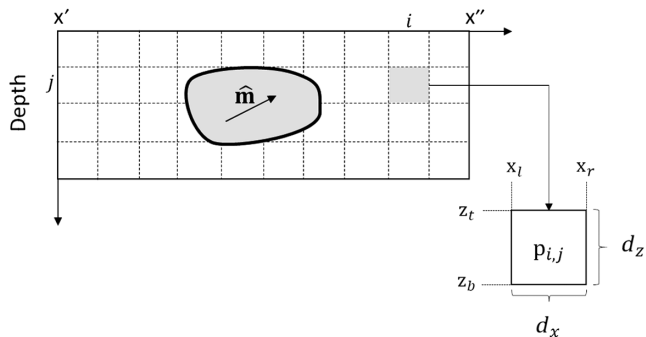


Figure 1. Model representation for a 2D magnetic body with uniform magnetization $\mathbf{M} = M\hat{\mathbf{m}}$: magnetic profile $X'-X''$ crossing the elongated source, regular mesh with $M = n_x \times n_z$ cells of size d_x and d_z (infinite along the y -axis). The cells have unknown magnetization intensities p_k but a constant magnetization direction $\hat{\mathbf{m}}$.

zation in the substrate can be represented by a mesh with $M = n_x \times n_z$ cells (Figure 1) of known size and position but unknown magnetization (intensity and direction).

The k th cell of the mesh $k = n_x(j - 1) + i$ has magnetization intensity p_k and inclination (projected at the x - z plane) I_k . A uniform body has constant p_k and I_k values for all cells. We regarded magnetic models with variable p_k , but inclination I_k , $k = 1:M$ equal to i_M . For igneous bodies, it is not a restrictive assumption given that the magnetization direction is frozen as the body cools below the critical temperature. The inclination i_M , defined by the unitary vector $\hat{\mathbf{m}}$, is the angle of the magnetization projected at the x - z plane. The anomalous vector field can be obtained from the horizontal \mathbf{f}_x and vertical \mathbf{f}_z components as

$$\mathbf{f}_t = \mathbf{f}_x \cos i_c + \mathbf{f}_z \sin i_c, \quad (1)$$

where i_c is the inclination of the local main field at the x - z plane. The i th entries in \mathbf{f}_x and \mathbf{f}_z can be evaluated from a mesh of prismatic bodies as

$$\begin{cases} f_{x,i}(\mathbf{p}, \hat{\mathbf{m}}) = \sum_{k=1:M} p_k f_{x,i,k}(\hat{\mathbf{m}}) \\ f_{z,i}(\mathbf{p}, \hat{\mathbf{m}}) = \sum_{k=1:M} p_k f_{z,i,k}(\hat{\mathbf{m}}) \end{cases}, \quad (2)$$

with $f_{x,i,k}(\hat{\mathbf{m}})$ expressing the x -component of the magnetic field evaluated at the i th profile point caused by the k th cell of the model with magnetization intensity p_k ; all cells of the model have the (unknown) magnetization direction $\hat{\mathbf{m}}$. The IAVF at the i th station is

$$f_i(\mathbf{p}) = [f_{x,i}(\mathbf{p}, \hat{\mathbf{m}})^2 + f_{z,i}(\mathbf{p}, \hat{\mathbf{m}})^2]^{\frac{1}{2}}, \quad (3)$$

explicitly suppressing magnetization direction $\hat{\mathbf{m}}$ given that the intensity field $f_i(\mathbf{p})$ is invariant with the magnetization direction for 2D sources. The IAVF can be evaluated using any direction $\hat{\mathbf{m}}$, for example, $\hat{\mathbf{m}} = \hat{\mathbf{t}}$. The sensitivity coefficients $f_{x,i,k}$ and $f_{z,i,k}$ can be stored to evaluate the model's response to minimize data fitting to IAVF according to a nonlinear problem. The ASA can be calculated from x - and z -derivatives applied to TFA as

$$\begin{cases} \frac{\partial f_{t,i}(\mathbf{p}, \hat{\mathbf{m}})}{\partial x} = \sum_{k=1:M} p_k \frac{\partial f_{t,i,k}(\hat{\mathbf{m}})}{\partial x} \\ \frac{\partial f_{t,i}(\mathbf{p}, \hat{\mathbf{m}})}{\partial z} = \sum_{k=1:M} p_k \frac{\partial f_{t,i,k}(\hat{\mathbf{m}})}{\partial z} \end{cases}, \quad (4)$$

where $f_{t,i,k}(\hat{\mathbf{m}})$ is the TFA evaluated from the k th cell of the model at the i th station of the profile. As in the case of the IAVF, the ASA is independent of magnetization direction $\hat{\mathbf{m}}$, such that $a_i(\mathbf{p}, \hat{\mathbf{m}}) \equiv a_i(\mathbf{p})$, with

$$a_i(\mathbf{p}) = \left[\left(\frac{\partial f_{t,i}(\mathbf{p}, \hat{\mathbf{m}})}{\partial x} \right)^2 + \left(\frac{\partial f_{t,i}(\mathbf{p}, \hat{\mathbf{m}})}{\partial z} \right)^2 \right]^{\frac{1}{2}}. \quad (5)$$

The sensitivity coefficients $h_{i,k}^x \equiv \partial f_{t,i,k}(\hat{\mathbf{m}}) / \partial x$ and $h_{i,k}^z \equiv \partial f_{t,i,k}(\hat{\mathbf{m}}) / \partial z$ can be evaluated with any $\hat{\mathbf{m}}$ (e.g., $\hat{\mathbf{m}} = \hat{\mathbf{t}}$) and stored to evaluate equation 4 during iterative procedures allowing nonlinear data fitting to ASA. The SF can be evaluated from IAVF and ASA (Tuma and Mendonça, 2007) as

$$s_i(\mathbf{p}_b) = \frac{a_i(\mathbf{p})}{f_i(\mathbf{p})}, \quad (6)$$

where \mathbf{p}_b is a binary version of vector \mathbf{p} , obtained by keeping the zeros for cells with magnetization intensity equal to zero and attributing 1 to cells with non-null entries. This binary property is intrinsic to 2D homogeneous sources given that the numerator and denominator in equation 6 are multiplied by a common factor (the magnetization intensity), which is canceled when divided. This allows data fitting to SF, assuming any values for magnetization direction $\hat{\mathbf{m}}$ and the same magnetization intensity for all cells in the mesh. The SF depends only on source geometry; thus, it is termed the “shape function.”

Figure 2 shows the processing flowchart scheme developed to obtain the SF from a set of TFA data. The processing flowchart applies a sequence of linear transformations in the Fourier domain (Blakely, 1996), available in most potential field processing packages.

Inverse problem

Finding a binary distribution that fits SF data is a difficult task because of the complexity of the objective functions that are minimized. To make matters worse, a solution exists only for homogeneous sources, but when analyzing a real data set no one can be sure if the observed fields arise from homogeneous sources or not. To circumvent this problem, we implemented a set of preliminary solutions fitting ASA-IAVF and then ASA-IAVF-SF according to the sequential procedure illustrated in Figure 3, postponing the inversion of SF data under a binary constraint. The existence of a solution in this later stage of the sequential inversion is indicative of a source with uniform magnetization (intensity and direction)

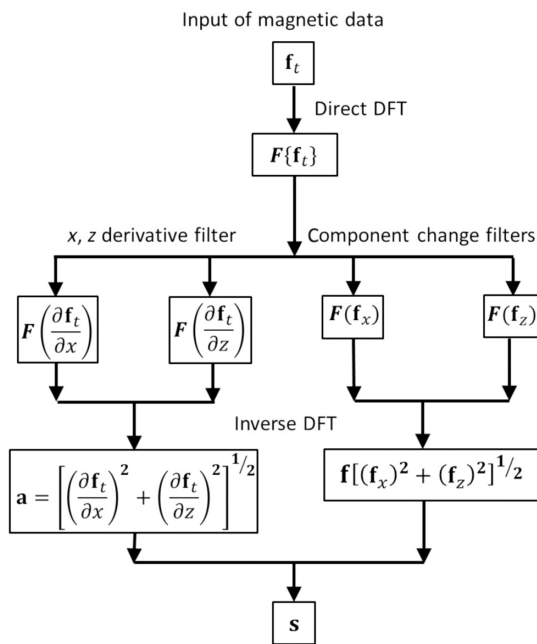


Figure 2. Processing flowchart for the inversion procedure and homogeneity testing: TFA \mathbf{f} , as input and filtering operations in the Fourier domain with the discrete Fourier transform (DFT). Processing products to be inverted: ASA \mathbf{a} , IAVF \mathbf{f} , SF \mathbf{s} . Field intensities \mathbf{a} and \mathbf{f} are invariant with the magnetization direction; SF is invariant with the magnetization direction and intensity.

even though these parameters are not determined explicitly at this stage. This can be done by using the binary solution to determine a scale factor fitting the ASA and/or IAVF, thus estimating the magnetization intensity. The magnetization inclination can be determined by fixing the shape and magnetization intensity while varying magnetization inclination to fit TFA.

As illustrated in Figure 3, the first step of our proposed sequential procedure jointly inverts the IAVF data set f_1^0, \dots, f_n^0 and the ASA data set a_1^0, \dots, a_n^0 by minimizing the objective function $\varphi_{f,a}(\mathbf{p})$:

$$\varphi_{f,a}(\mathbf{p}) = \frac{1}{nR_f} \sum_{i=1:n} [f_i^o - f_i(\mathbf{p})]^2 + \frac{1}{nR_a} \sum_{i=1:n} [a_i^o - a_i(\mathbf{p})]^2 + \frac{\mu_s}{M} \sum_{i=1:M} p_i^2. \quad (7)$$

The joint minimization of IAVF and ASA enhances the model sensitivity with depth, by incorporating the IAVF sensitivity to deeper levels with ASA sensitivity to shallower levels (Liu et al., 2013, 2015). The terms R_f and R_a are scaling factors (IAVF and ASA peak amplitudes) to balance the contributions to each field in the joint data fitting. The i th entry p_i of the M -dimensional vector \mathbf{p} assigns the magnetization intensity for the mesh i th cell. The third addend in equation 7 implements the zeroth-order Tikhonov regularization (Tikhonov and Arsenin, 1977) with global smoothness

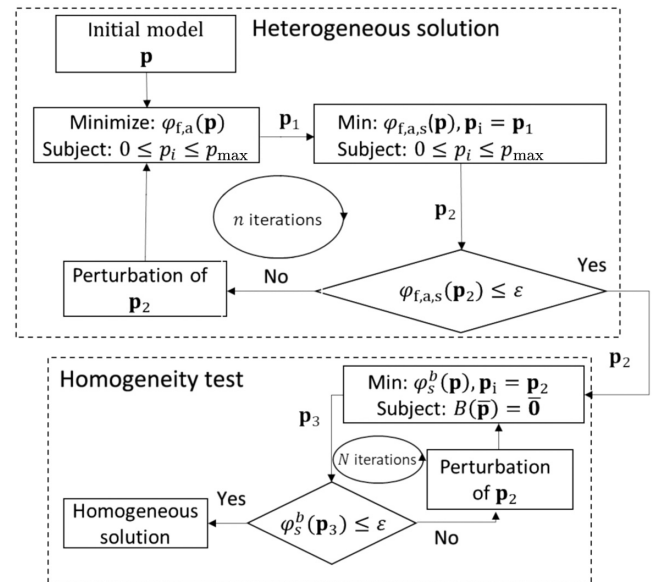


Figure 3. Flowchart for magnetic data inversion and homogeneity test. Upper block: procedure to obtain a heterogeneous solution, starting with the minimization of $\varphi_{f,a}$ by fitting \mathbf{f} and \mathbf{a} , to provide solution \mathbf{p}_1 that serves as the initial solution to a second stage, where $\varphi_{f,a,s}$ is minimized. In the second stage, \mathbf{f} , \mathbf{a} , and \mathbf{s} are inverted to find solution \mathbf{p}_2 . The upper block output (solution \mathbf{p}_2) is subjected to the homogeneity test by minimizing φ_s subject to the binary constraint $B(p_i) = 0$ for each i th entry in \mathbf{p} , as in equation 11. A solution \mathbf{p}_3 such that $\varphi_s(\mathbf{p}_3) \approx \varphi_s(\mathbf{p}_2) \leq \epsilon$ is indicative that the analyzed data set that can be associated to a model with uniform magnetization (inclination and intensity). In both blocks, random perturbations in temporary solutions are repeated (n iterations or N iterations) to improve convergence. Random perturbations are applied to the compact solution \mathbf{p}_2 when starting a new minimization round after convergence is not obtained.

(Barbosa et al., 1997). The positive scalar μ_s establishes a threshold between goodness in data fitting and smoothness for the magnetization distribution. The solution \mathbf{p}_1 minimizing $\varphi_{f,a}(\mathbf{p})$ is fed as an initial solution to minimize

$$\varphi_{f,a,s}(\mathbf{p}) = \frac{1}{nR_f} \sum_{i=1:n} [f_i^o - f_i(\mathbf{p})]^2 + \frac{1}{nR_a} \sum_{i=1:n} [a_i^o - a_i(\mathbf{p})]^2 + \frac{1}{nR_s} \sum_{i=1:n} [s_i^o - s_i(\mathbf{p})]^2 + \frac{\mu_c}{M} \sum_{i=1:M} p_i r_i, \quad (8)$$

which in addition to fitting IAVF and ASA also fits SF data s_1^0, \dots, s_n^0 (R_s as the SF peak amplitude). The fourth term of functional $\varphi_{f,a,s}(\mathbf{p})$ weights the model parameters with

$$r_i = \frac{p_i}{p_i^2 + \alpha^2}, \quad (9)$$

which suits solutions with compacity (Last and Kubik, 1983; Barbosa and Silva, 1994; Portniaguine and Zhdanov, 2002). A sufficiently small scalar α prevents division by zero; a positive scalar μ_c balances the compacity degree with the data fitting quality. The minimization of $\varphi_{f,a}$ is usually fast but its output does not necessarily fit $\varphi_{f,a,s}$, thus the need for a second step to fit SF with the compacity constraint as in equation 9. The interval constraint $0 \leq p_k \leq p_{\max}$ is incorporated to guarantee positivity and an upper bound p_{\max} according to the magnetization intensity values for the rocks in the region under study. The minimization of functionals $\varphi_{f,a}$ and $\varphi_{f,a,s}$ with interval constraints was implemented with the interior point method (Byrd et al., 1999) as coded in the FMINCON function of the MATLAB optimization package.

Homogeneity test

Preliminary solutions sequentially minimizing $\varphi_{f,a}$ and $\varphi_{f,a,s}$ provide a trial solution \mathbf{p}_3 (as illustrated in Figure 3) that is subject to the uniformity test. This is done by minimizing

$$\varphi_s^b(\mathbf{p}) = \frac{1}{nR_s} \sum_{i=1:n} [s_i^o - s_i(\mathbf{p})]^2, \quad (10)$$

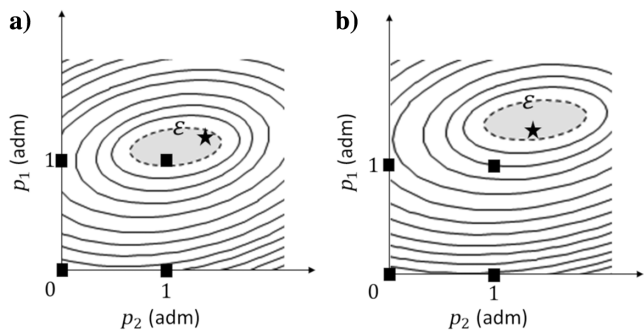


Figure 4. Illustration of compact solution \mathbf{p}_2 (star) and binary solution (square) \mathbf{p}_3 as a set of alternative solutions, similarly allowing fitness to SF data below the error margin ϵ . Schematics for a fictitious model with two parameters only (p_1 and p_2). In case (a), a uniformly magnetized body can be associated with the modeled fields. In case (b), a uniformly magnetized body cannot be associated with the modeled fields because the binary solution does not allow data fitness below ϵ .

subject to the equality constraint $B(p_i) = 0$ for $i = 1:n$, such that

$$B(p_i) \equiv \sum_{i:M} (p_i - p_i r_i)^2, \quad (11)$$

where the term r_i is expressed in equation 9. Note that condition $B(p_i) = 0$ for $i = 1:n$ holds only when the entries in the testing parameters \mathbf{p} assume values of 0 or 1 (supposing that α in equation 9 is set sufficiently small), hence the term “binary solution.” Binary solutions are described in several papers (Portniaguine and Zhdanov 2002; Krahenbuhl and Li, 2006; Van Zon and Roy-Chowdhury, 2006; Li et al., 2018), usually representing the model parameter as a product of a binary distribution with a scale factor representing the magnetization intensity or the density contrast for gravity fields. In minimizing SF as in equations 10 and 11, no assumption about a known scaling factor is required. The sequence of mesh cells with 1 and 0 outlines the shape of the true sources without any assumption about their magnetization intensity and direction.

We can verify if a given 2D magnetic field can be associated with a body with uniform magnetization, if a binary solution \mathbf{p}_3 minimizing φ_s^b (equation 10) provides comparable data fitting as the solution \mathbf{p}_2 minimizing $\varphi_{f,a,s}$ (equation 8). In summary, \mathbf{p}_2 and \mathbf{p}_3 must be such that $\varphi_s(\mathbf{p}_2) \approx \varphi_s(\mathbf{p}_3) \leq \epsilon$, with φ_s representing the least-squares measure in fitting SF. Figure 4 illustrates the solutions \mathbf{p}_2 and \mathbf{p}_3 as a set of alternative solutions, similarly allowing SF data fitting below the margin of error defined by ϵ . In this figure, two model solutions are represented. The first one (the star) is the solution \mathbf{p}_2 associated with a nonuniform magnetization model but fitting ASA, IAVF, and SF. The second solution (marked with a square) also minimizes φ_s but is constrained to achieve only 0 or 1 values (the binary constraint). Figure 4a represents a binary solution such that $\varphi_s(\mathbf{p}_2) \approx \varphi_s(\mathbf{p}_3) \leq \epsilon$ as expected when a uniformly magnetized body can be associated with the modeled fields. Alternately, in Figure 4b, the binary solution fits the SF function with residuals higher than the threshold ϵ , suggesting that a binary model must be rejected as a possible solution because it provides no fitness to the observed data. In addition to parameter ϵ to account for the data fitness, one can use the coefficient $R^2 = 1 - [\sum_{i=1}^n (y_i - y_{i,c})^2 / \sum_{i=1}^n (y_i - \hat{y}_i)^2]$ to compare data fitting provided by solutions \mathbf{p}_2 and \mathbf{p}_3 . In this expression, y_i and $y_{i,c}$ are observed and model the evaluated data and \hat{y}_i models the mean of the observed data. The R^2 parameter varies within 0 and 1, with values close to 1 usually identifying an overall data fitting between the observed and measured data. The parameter ϵ must satisfy $\varphi_s(\mathbf{p}_2) \approx \varphi_s(\mathbf{p}_3) \leq \epsilon$, and, in practice, it can be set as the data fitness level provided by the stable and compact solution \mathbf{p}_2 . The use of solution \mathbf{p}_2 as an initial solution in searching solution \mathbf{p}_3 tends to enforce convergence because the compact and binary solutions share many zeros as a common property.

In essence, the finding of a binary solution such that $\varphi_s(\mathbf{p}_3) > \epsilon$ indicates that no solution with uniform magnetization can be associated with the observed data set. Otherwise, the finding of a solution such that $\varphi_s(\mathbf{p}_3) \leq \epsilon$ indicates that a uniform magnetization can be associated with the analyzed data. In the first case $\varphi_s(\mathbf{p}_3) > \epsilon$, the existence of a uniform distribution must be discarded; in the second case, it can be regarded as a possible representation for the underlying sources. The homogeneity test then consists of verifying the existence of a binary solution \mathbf{p}_3 using as the starting point the compact solution \mathbf{p}_2 . The need to use the

compact solution \mathbf{p}_2 as a trial solution intends to enforce convergence in minimizing $\phi_s^b(\mathbf{p})$ to obtain solution \mathbf{p}_3 .

NUMERICAL SIMULATIONS

Numerical simulation tests aim to evaluate the ability of our proposed procedure to delineate the source geometry and determine if the magnetization condition is uniform or not. In all of the tested models, synthetic data for IAVF, ASA, and SF were contaminated with pseudorandom Gaussian noise with zero mean and a standard deviation of 3% of the respective amplitude values. Two cases were tested by simulating bodies with the same geometry, but with uniform and nonuniform magnetization.

Dipping body models

Models in Figure 5 simulate dipping bodies with geometry similar to a model tested by Liu et al. (2015). Model A represents a homogeneous body with magnetization of 1 Am^{-1} , comprising seven juxtaposed prisms. Each prism is 50 m in width; the shallower portion is 150 m deep, and the deeper one occurs at a depth of 350 m. Model B has the same geometry, but with its southern (shallower) portion with a magnetization of 2 Am^{-1} . Model B is then composed by groups of prisms with the magnetization intensity of 1 and 2 Am^{-1} , thus simulating a model with variable magnetization intensity. The local main field inclination is 60° , and the declination is 0° . The subsurface was divided into $M = 800$ cells ($n_x = 40, n_z = 20$) of size $25 \times 25 \text{ m}$. For model A, the interval constraint was set to $0 \leq p_k \leq 2 \text{ Am}^{-1}$ and the regularization parameters were $\mu_s = 1$ and $\mu_c = 1$. For model B, the interval constraint was set to $0 \leq p_k \leq 4 \text{ Am}^{-1}$ with regularization parameters of $\mu_s = 10^{-3}$ and $\mu_c = 1$.

As shown in Figure 5, all of the field quantities (IAVF, ASA, and SF) for model A were fitted accordingly by the model obtained from data inversion. Solution \mathbf{p}_2 resulted from inverting IAVF-ASA-SF; solution \mathbf{p}_3 satisfies the binary constraint for uniformity. As shown in Figure 6a, both solutions allowed data fitting with a coefficient R^2 higher than 0.98, thus indicating that the respective IAVF, ASA, and SF can be regarded as associated with a uniformly magnetized body. In a practical situation, because two solutions explain the same data set, the interpreter should weigh the available geologic information to accept one of the models as a more plausible one. Model B, however, failed the uniformity test. Its R^2 parameter (Figure 6b) dropped from as high as 0.98 for the unconstrained solution to as low as 0.59 for the binary solution. This degrading of the data fitness represents a solution as in the schematics shown in Figure 4b, showing that no solution suited with a binary distribution was able to represent the measured data set. The

higher magnetized bodies at the southern side of the profile are recognized by solution \mathbf{p}_2 , which gives a binary solution \mathbf{p}_3 that is unable to fit the associated data set below the same error margin. In summary, the uniformity test is based on how far the data fitness is degraded when the binary constraint is applied. The reference to check the data fitness quality is the one provided by solution \mathbf{p}_2 , which means a stable solution satisfying interval constraints for physical properties and general attributes of smoothness and compactness expected from geologic entities.

REAL DATA APPLICATION

We applied our technique to interpret a magnetic north-south profile 4050 m long, acquired in the northeastern border of the

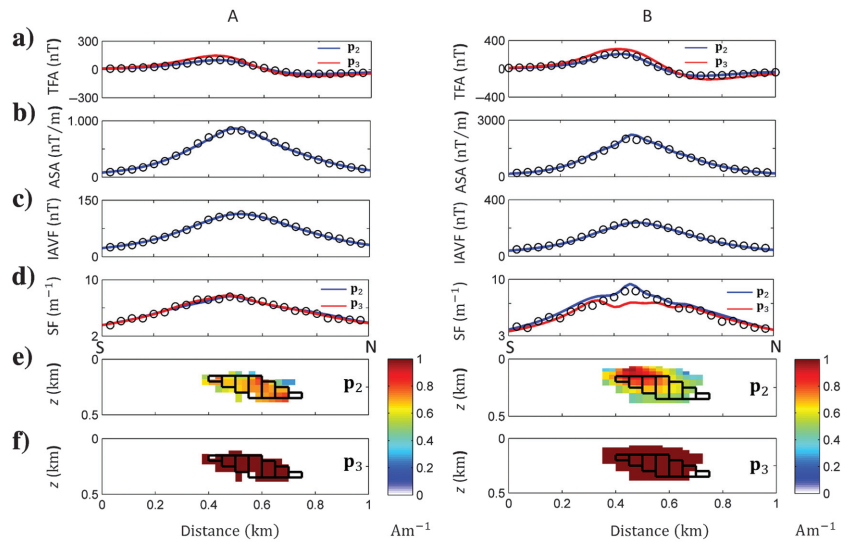


Figure 5. Numerical simulation with uniform (model A) and nonuniform (model B) representing dipping geological structures: (a) synthetic noisy data (circles) and data fitting from models \mathbf{p}_2 and \mathbf{p}_3 (lines) to the TFA, (b) IAVF, (c) ASA, and (d) SF. The magnetization model in (e) is the compact solution \mathbf{p}_2 . The magnetization model in (f) satisfies the binary constraint.

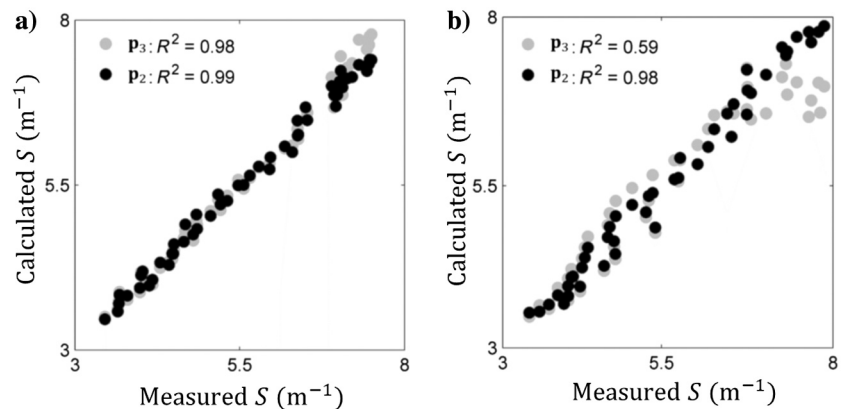


Figure 6. Crossplot of the measured (synthetic data) and evaluated SF from \mathbf{p}_2 (non-uniform magnetization) and \mathbf{p}_3 (binary, uniform magnetization), and the respective R^2 parameter. For the uniform body (model A), the R^2 coefficient is as good as that for models \mathbf{p}_2 and \mathbf{p}_3 . For the variable magnetization body (model B), the data fitness under the binary constraint (solution \mathbf{p}_3) degrades and parameter R^2 drops from 0.98 to 0.59, thus recognizing the variation of magnetization in model B.

Paraná Basin, Brazil. This part of the basin is comprised of Paleozoic sediments intruded by sills and dikes of diabase of the Cretaceous Serra Geral Formation (Hawkesworth et al., 1992). This formation comprises flood basalts, sills, and dikes developed in the early stages of the South Atlantic opening (White and McKenzie, 1989). The magnetic anomaly and IAVF, ASA, and SF were presented by Tuma and Mendonça (2007) when modeling the magnetic sources with a set of juxtaposed prisms with their tops at the ground surface and of unknown thickness. This representation is less effective in mapping the magnetization distribution because uniform domains were assumed from top to bottom. We reinterpreted this data set using a mesh model of cells capturing magnetization variations in two directions. The subsurface was divided into $M = 156$ mesh cells ($n_x = 26 \times n_z = 6$) with a size of 162×80 m. The interval constraint was set to $0 \leq p_k \leq 5 \text{ Am}^{-1}$ with regularization parameters of $\mu_s = 10^{-3}$ and $\mu_c = 10^{-3}$.

The inverted models are shown in Figure 7. The solution \mathbf{p}_2 satisfactorily fits fields IAVF, ASA, and SF and represents the magnetic structure as two nonconnected magnetic bodies. The inverted distribution captures the same trends formerly outlined by Tuma and Mendonça (2007) but suggests that the bodies are disjointed and packed into two domains.

As shown in Figure 8, the R^2 coefficient drops from 0.94 for solution \mathbf{p}_2 to 0.26 for solution \mathbf{p}_3 satisfying the binary constraint, indicating bodies with variable magnetization. But because two bodies are outlined, the condition of nonuniform magnetization could apply to either bodies forming two homogeneous domains or bodies with internal variations in magnetization intensity. The

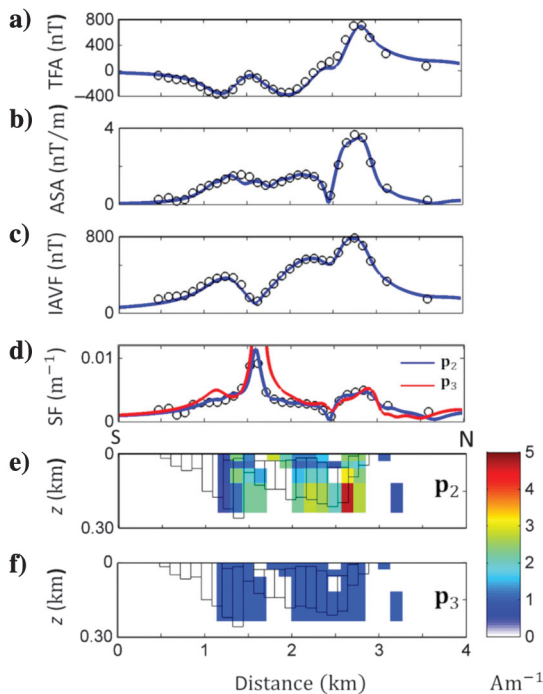


Figure 7. Real data application with a ground magnetic profile across intrusive diabase bodies: (a) data fitness to the TFA, (b) fitness to ASA, (c) fitness to IAVF, and (d) fitness to SF. (e) Solution \mathbf{p}_2 and (f) solution \mathbf{p}_3 satisfying the binary constraint. Panel (d) was intentionally cut off to make clear the data fitness provided by solution \mathbf{p}_2 (the blue curve). In the black vertical prisms are the solution from Tuma and Mendonça (2007).

first hypothesis can be tested by taking into account the average magnetization of the two bodies outlined in solution \mathbf{p}_2 .

As shown in Figure 9, the mean values for the southern and northern bodies are about 2.0 ± 0.4 and $2.4 \pm 0.8 \text{ Am}^{-1}$, respectively. Next, we evaluated the SF from a model derived from solution \mathbf{p}_2 by assigning values equal to 1 for the southern body and equal to 1.2 for the northern body, thus keeping the proportion 2.4/2.0 for their mean values. This gives the model shown in Figure 10, providing acceptable data fitting with R^2 of 0.86. These results indicate that the diabase bodies intruding the sediments in the studied area can be characterized as being comprised of two uniform entities: one with magnetization 20% higher than the other. By fitting ASA and IAVF with this “modified binary” model (i.e., comprised of zeros, 1.0, and 1.2) the magnetization intensity was estimated as 2.0 and 2.4 Am^{-1} , respectively. The scaling factor equal to 2.0 was determined by matching the amplitude of the measured intensity fields with those evaluated from the model with

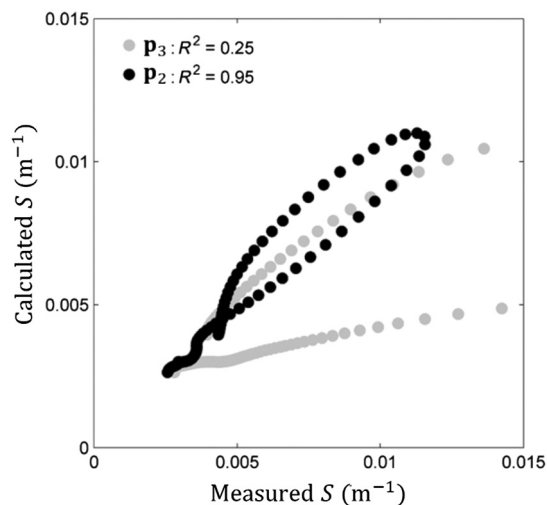


Figure 8. Crossplot of measured and evaluated SF for solutions \mathbf{p}_2 and \mathbf{p}_3 .

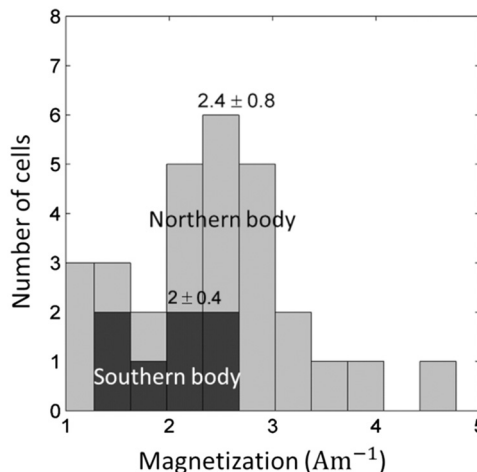


Figure 9. Histogram of magnetization values for cells covering the bodies in the northern and southern portions of the profile: the southern body with a mean value of $2.0 \pm 0.4 \text{ Am}^{-1}$; the northern body with a mean value of $2.4 \pm 0.8 \text{ Am}^{-1}$.

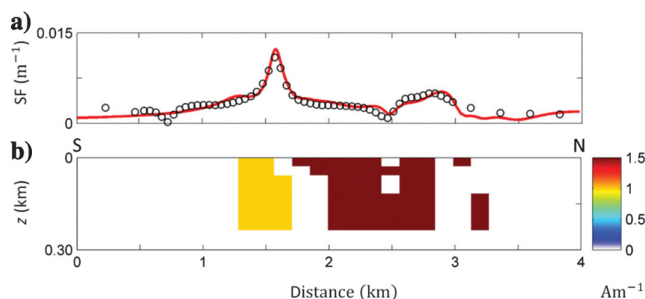


Figure 10. Model with approximated binary solution with values equal to 1.0 (the southern body) and 1.2 (the northern body), and the corresponding SF fitting curve (the line in red) to observed data (the circles).

nonzero terms equal to 1.0 or 1.2. Fitting to the magnetic anomaly was accomplished by setting a magnetization inclination of -50° for the two bodies, as inferred by Tuma and Mendonça (2007). In sharing magnetization inclination, the two bodies can be regarded as emplaced when the geomagnetic field was at the normal position but in higher magnetic latitude because the inclination of the present field is -30° .

CONCLUSION

We have developed a sequential procedure that facilitates the convergence of the nonlinear inversion of a ratioed quantity involving field intensities and developed a procedure to verify if the assumption about homogeneous magnetization holds. The heterogeneous magnetization model is recovered by minimizing quantities invariant with the magnetization direction (IAVF and ASA). These quantities, in addition to SF, are invariant with the magnetization intensity. The model was subjected to a uniformity test looking for a solution of zeros and ones that minimizes the SF. Degrading of data fitting under the binary constraint is indicative of heterogeneously magnetized bodies. A solution, otherwise satisfying the binary condition, identifies a homogeneously magnetized source. The geometry of the source is outlined by the binary solution and, by sequentially fitting the intensity fields (ASA, IAVF) and the TFA, the magnetization intensity and direction are determined. This procedure, when applied to a ground magnetic anomaly along a profile crossing an intrusive body of diabase, revealed the existence of two disjointed but homogeneous bodies, one of them with a magnetization 20% higher than the other, both entities with the same magnetization direction. We stress the importance of such findings in characterizing an igneous body under a sequential inverse approach and the application of the uniformity test to better outline structures and physical properties of underlying magnetic bodies. The homogeneity test can be applied only for 2D magnetic anomalies for which the related intensity fields are invariant with the magnetization direction.

ACKNOWLEDGMENTS

Inputs from E. Gasperikova and three anonymous reviewers substantially improved this contribution. This study was financed in part by the Coordenação de Aperfeiçoamento de Pessoal de Nível Superior – Brasil (CAPES) (Finance Code 001).

DATA AND MATERIALS AVAILABILITY

Data associated with this research are available and can be obtained by contacting the corresponding author.

REFERENCES

- Barbosa, V. C. F., and J. B. C. Silva, 1994, Generalized compact gravity inversion: *Geophysics*, **59**, 57–68, doi: [10.1190/1.1443534](https://doi.org/10.1190/1.1443534).
- Barbosa, V. C. F., J. B. C. Silva, and W. E. Medeiros, 1997, Gravity inversion of basement relief using approximate equality constraints on depths: *Geophysics*, **62**, 1745–1757, doi: [10.1190/1.1444275](https://doi.org/10.1190/1.1444275).
- Blakely, R. J., 1996, *Potential theory in gravity and magnetic applications*: Cambridge University Press.
- Byrd, R. H., M. E. Hribar, and J. Nocedal, 1999, An interior point algorithm for large-scale nonlinear programming: *SIAM Journal on Optimization*, **9**, 877–900, doi: [10.1137/S1052623497325107](https://doi.org/10.1137/S1052623497325107).
- Hawkesworth, C., K. Gallagher, S. Kelly, M. S. Mantovani, D. Peate, M. Regelous, and N. Rogers, 1992, Paraná magmatism and the opening of the south Atlantic: Geological Society, London, Special Publications, **68**, 221–240, doi: [10.1144/GSL.SP.1992.068.01.14](https://doi.org/10.1144/GSL.SP.1992.068.01.14).
- Hidalgo-Gato, M. C., and V. C. F. Barbosa, 2015, Edge detection of potential-field sources using scale-spacemongenic signal: *Fundamental principles: Geophysics*, **80**, no. 5, J27–J36, doi: [10.1190/geo2015-0025.1](https://doi.org/10.1190/geo2015-0025.1).
- Krahenbuhl, R. A., and Y. Li, 2006, Inversion of gravity data using a binary formulation: *Geophysical Journal International*, **167**, 543–556, doi: [10.1111/j.1365-246X.2006.03179.x](https://doi.org/10.1111/j.1365-246X.2006.03179.x).
- Last, B. J., and K. Kubik, 1983, Compact gravity inversion: *Geophysics*, **48**, 713–721, doi: [10.1190/1.1441501](https://doi.org/10.1190/1.1441501).
- Li, X., and M. Pilkington, 2016, Attributes of the magnetic field, analytic signal, and monogenic signal for gravity and magnetic interpretation: *Geophysics*, **81**, no. 6, J79–J86, doi: [10.1190/geo2015-0697.1](https://doi.org/10.1190/geo2015-0697.1).
- Li, Y., S. Shearer, M. Haney, and N. Dannemiller, 2010, Comprehensive approaches to 3D inversion of magnetic data affected by remanent magnetization: *Geophysics*, **75**, no. 1, L1–L11, doi: [10.1190/1.3294766](https://doi.org/10.1190/1.3294766).
- Li, Z., C. Yao, Y. Zheng, J. Wang, and Y. Zhang, 2018, 3D magnetic sparse inversion using an interior point method: *Geophysics*, **83**, no. 3, J15–J32, doi: [10.1190/geo2016-0652.1](https://doi.org/10.1190/geo2016-0652.1).
- Liu, S., X. Hu, T. Liu, J. Feng, W. Gao, and L. Qiu, 2013, Magnetization vector imaging for bore hole magnetic data based on magnitude magnetic anomaly: *Geophysics*, **78**, no. 6, D429–D444, doi: [10.1190/geo2012-0454.1](https://doi.org/10.1190/geo2012-0454.1).
- Liu, S., X. Hu, Y. Xi, T. Liu, and S. Xu, 2015, 2D sequential inversion of total magnetic and total magnetic anomaly data affected by remanent magnetization: *Geophysics*, **80**, no. 3, K1–K12, doi: [10.1190/geo2014-0019.1](https://doi.org/10.1190/geo2014-0019.1).
- Mendonça, C. A., 2004, Inversion of gravity-field inclination to map the basement relief of sedimentary basins: *Geophysics*, **69**, 1240–1251, doi: [10.1190/1.1801940](https://doi.org/10.1190/1.1801940).
- Portmiguine, O., and M. S. Zhdanov, 2002, 3-D magnetic inversion with data compression and image focusing: *Geophysics*, **67**, 1532–1541, doi: [10.1190/1.1512749](https://doi.org/10.1190/1.1512749).
- Salem, A., S. Williams, D. Fairhead, R. Smith, and D. Ravat, 2008, Interpretation of magnetic data using tilt-angle derivatives: *Geophysics*, **73**, no. 1, L1–L10, doi: [10.1190/1.2799992](https://doi.org/10.1190/1.2799992).
- Shearer, S., and Y. Li, 2004, 3D inversion of magnetic total gradient data in the presence of remanent magnetization: 74th Annual International Meeting, SEG, Expanded Abstracts, 774–777, doi: [10.1190/1.1851318](https://doi.org/10.1190/1.1851318).
- Silva, J. B. C., W. E. Medeiros, and V. C. F. Barbosa, 2001, Potential-field inversion: Choosing the appropriate technique to solve a geologic problem: *Geophysics*, **66**, 511–520, doi: [10.1190/1.1444941](https://doi.org/10.1190/1.1444941).
- Stavrev, P., 2006, Inversion of elongated magnetic anomalies using magnitude transforms: *Geophysical Prospecting*, **54**, 153–166, doi: [10.1111/j.1365-2478.2006.00528.x](https://doi.org/10.1111/j.1365-2478.2006.00528.x).
- Stavrev, P., and D. Gerovska, 2000, Magnetic field transforms with low sensitivity to the direction of source magnetization and high centrality: *Geophysical Prospecting*, **48**, 317–340, doi: [10.1046/j.1365-2478.2000.00188.x](https://doi.org/10.1046/j.1365-2478.2000.00188.x).
- Tikhonov, A. N., and V. Y. Arsenin, 1977, *Solutions of ill-posed problems*: W. H. Winston & Sons.
- Tuma, S. L., and C. A. Mendonça, 2007, Stepped inversion of magnetic data: *Geophysics*, **72**, no. 3, L21–L30, doi: [10.1190/1.2711661](https://doi.org/10.1190/1.2711661).
- Van Zon, T., and K. Roy-Chowdhury, 2006, Structural inversion of gravity data using linear programming: *Geophysics*, **71**, no. 3, J41–J50, doi: [10.1190/1.2197491](https://doi.org/10.1190/1.2197491).
- White, R., and D. McKenzie, 1989, Magmatism at rift zones: The generation of volcanic continental margins and flood basalts: *Journal of Geophysical Research*, **94**, 7685–7729, doi: [10.1029/JB094iB06p07685](https://doi.org/10.1029/JB094iB06p07685).
- Wijns, C., C. Perez, and P. Kowalczyk, 2005, Theta map: Edge detection in magnetic data: *Geophysics*, **70**, no. 4, L39–L43, doi: [10.1190/1.1988184](https://doi.org/10.1190/1.1988184).

Biographies and photographs of the authors are not available.